Nucleic Acids Research, 2005, Vol. 33, No. 7 ***e69***
doi:10.1093/nar/gni067

Surface plasmon field-enhanced fluorescence spectroscopy studies of primer extension reactions

Gudrun Stengel* and Wolfgang Knoll

Max-Planck-Institute for Polymer Research, Ackermannweg 10, D-55128 Mainz, Germany

Received January 18, 2005; Revised and Accepted March 29, 2005

ABSTRACT

Surface plasmon field-enhanced fluorescence spectroscopy (SPFS) utilizes the evanescent electromagnetic field of a surface plasmon to excite chromophors in close proximity to the surface. While conventional surface plasmon resonance spectroscopy allows the observation of surface reactions by means of refractive index changes, SPFS additionally provides a channel for the read-out of fluorescence changes. Thus, the detection limit for low mass compounds, whose adsorption is only accompanied by small refractive index changes, can be substantially improved by fluorescent labeling. In this study, we present the first example that utilizes SPFS to follow the dynamics of an enzymatic reaction. The elongation of surface-tethered DNA has been observed by the incorporation of Cy5-labeled nucleotides into the nascent strand by the action of DNA polymerase I (Klenow fragment). The technique offers a rapid way to determine the binding constant and the catalytic activity of a DNA processing enzyme, here exemplified by the Klenow fragment. Furthermore, the effect of mispaired bases in the primer/template duplex and the influence of different label densities have been studied. The resulting sensitivity for nucleotide incorporation, being in the femtomolar regime, combined with the specificity of the enzyme for fully complementary DNA duplexes suggest the application of this assay as a powerful tool for DNA detection.

INTRODUCTION

DNA polymerases have emerged as important biotechnological tools for the *in vitro* synthesis of double-stranded DNA. They are the key enzymes in PCR-based methods aiming at the detection of single point mutation (1,2) and in DNA sequencing procedures (3–5). Methods that utilize specific enzyme functions to prove the identity of a base sequence, such as DNA ligation (6), digestion (7), restriction (8) and primer extension (9), are generally more sensitive to base aberrations than those based on DNA hybridization reactions alone (10). The current trend aims at miniaturizing these enzyme-mediated assays into high-throughput compatible chip-formats, which reduces the amount of required analyte DNA and hence, improves the sensitivity limits and operational capacity. While DNA microarrays are commonly analyzed by measuring end-point fluorescence intensities, the surface attachment of reaction compounds has also encouraged the use of surface-sensitive physical detection principles. Typical examples are real-time methods such as surface plasmon resonance (SPR) (11–15) and quartz crystal microbalance (QCM) (16), both of which have been used for the studies of DNA and RNA polymerase action. These methods are more versatile than the conventional DNA microarrays as they provide access to reaction kinetics and hence, they give fundamental insights into the dynamics of enzyme–DNA interaction. Although SPR spectroscopy and QCM have been proven to be effective in monitoring DNA synthesis, they are not capable of detecting single nucleotide incorporation events owing to the small corresponding mass changes.

In this study, we report the use of surface plasmon field-enhanced fluorescence spectroscopy (SPFS) to monitor the incorporation of fluorescently labeled nucleotides into surface-attached oligonucleotides by the catalytic action of DNA polymerase I (Klenow fragment). In SPFS, the excitation of surface-confined chromophors is achieved by the evanescent electromagnetic field of a surface plasmon mode propagating along a gold–water interface. The conditions for the resonant excitation of surface plasmons strongly depend on the interfacial refractive index and can be matched by fine-tuning the incidence angle of the excitation light. At resonance, the interfacial evanescent field is enhanced by a factor of 16 (for a

*To whom correspondence should be addressed. Tel: +1 858 784 9046; Fax; +1 858 784 9067; Email: stengel@scripps.edu
Present address:
Gudrun Stengel, The Scripps Research Institute, 10550 North Torrey Pines Road, La Jolla, CA 92037, USA

gold–water interface at $\lambda = 633$ nm) relative to the incoming light. Its strength is maximal at the interface, and decays exponentially normal to the surface with a penetration depth, L_z, of ~150 nm. The large field enhancement is the basis underlying the excellent sensitivity of SPFS to the presence of fluorophores within the evanescent field, and which distinguishes it from total internal reflection fluorescence (TIRF) microscopy, which basically utilizes the same optical excitation geometry but operates without a metal surface and thus with much lower field enhancement.

Since introduced in 1999 (17), the merit of SPFS has been demonstrated in the studies of DNA duplexes with single base mismatches (18,19) and the detection of antibodies with attomolar sensitivity (20,21). Recent examples for other evanescent field fluorescent techniques that were used to monitor DNA polymerase and telomerase action are super critical angle fluorescence (SAF) detection (22,23), optical fibers (24), zero-mode waveguides (25) and a mini-DNA sequencing concept based on the single molecule fluorescence microscopy (26). In the present work, we have derived binding and catalytic constants for the KF by using SPFS, with particular focus on the merit of the primer extension reaction for the sensitive detection of single base point mutation and the added value obtained by probing interfacial reflectivity and fluorescence changes simultaneously.

MATERIALS AND METHODS

Instruments

A schematic representation of an SPFS set-up is depicted in Figure 1. The beam of a HeNe laser (Uniphase, 5 mW, $\lambda = 632.8$ nm) is modulated through a chopper that is connected to a login amplifier (EG&G). Then the beam passes through two polarizers (Glan-Thompson), which are used to adjust the polarization and the intensity of the laser beam. A programmable shutter blocks the beam constantly and is only opened for the purpose of data recording, which prevents the chromophores from photobleaching. As the laser beam hits the base of the coupling prism (Schott, LASFN9) it is reflected in an angle of 90° towards the photodiode. The prism is mounted on a flow cell (volume ~60 µl), which is part of a pump driven closed circulation system. The fluorescence emission of the sample is collected from the backside of the prism by a photomultiplier tube (PMT) (Hamamatsu), which is connected with a photon counter unit (Agilent). Before the beam reaches the PMT, it is focused through a lens ($f = 50$ mM; Owis) and passes an interference filter ($\lambda = 670$ nm, $\Delta\lambda = 10$ nm, LOT). If needed, the fluorescence light was attenuated with a 1.3 dB neural filter to keep the intensity within the region of linear response of the PMT. The fluorescence detection unit is mounted on the goniometer rotating together with the prism (sample) at θ, while the photodiode, recording the intensity of the reflected beam, rotates at 2θ.

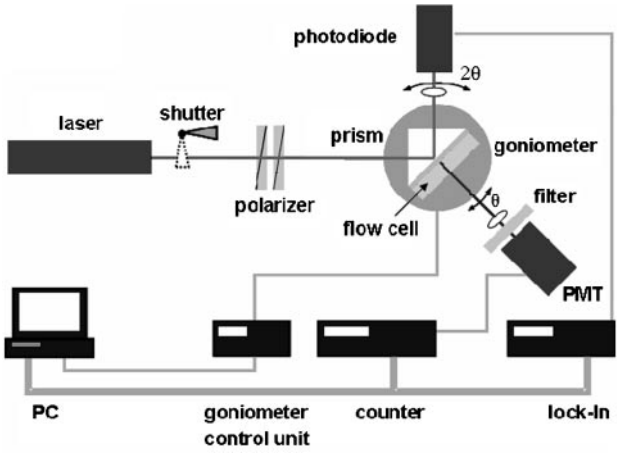

Figure 1. Scheme of the SPFS set-up.

Surface preparations

Clean LASFN9 glass slides ($n = 1.85$ at $\lambda = 633$ nm; Schott) were coated with a 50 nm gold layer using thermal evaporation (commercial apparatus from Edwards). The gold surface was functionalized using a binary self-assembled monolayer (SAM) of a long-chain thiol modified with a biotin end group [11-mercapto-(8-biotinamido-4,7,dioxaoctyl-)-undecanoylamide (27,28)] and 1-mercapto-undecanol (Sigma-Aldrich) at a ratio of 1:9 in absolute ethanol (total concentration 0.5 mM). The gold slides were incubated *ex situ* for 1 h, rinsed with ethanol, dried in a stream of nitrogen and mounted into the flow cell. Binding of streptavidin (Roche, Germany) to the thiol SAM was carried out *in situ* in physiological phosphate buffered saline buffer [10 mM phosphate buffer, 2.7 mM KCl and 150 mM NaCl (pH 7.4), tablets from Sigma-Aldrich]. Buffers were always degassed and supplemented with 0.005% (v/v) Tween-20 (Sigma-Aldrich). This step was followed by the immobilization of a 5′-biotinylated primer strand and the subsequent hybridization of a template strand. The template strands were phosphorylated at the 3′ terminus in order to inhibit the polymerase reaction at this site. All oligonucleotides were purchased from MWG Biotech (Germany) and were dissolved in HSM buffer at 1 µM concentration (10 mM HEPES, 150 mM NaCl and 10 mM $MgSO_4$). Depending on the objective of the experiment, the following primers and template strands were combined to form duplexes (the duplexes are named as primer/template).

Primers: 5′-Biotin-$(TTT)_5$**ACG TCA GTC TCA CCC**-3′ (**P45**); 5′-Biotin-$(TTT)_5$**ACG TCA GTC TCA CCG**-3′ (**P45tmm**); and 5′-Biotin-$(TTT)_5$**ACG TCA GTC TCA GCC**-3′ (**P45imm**).

Templates and targets: 5′-AGT TAC AGA GGT AGT AGT GGC TGA GTG AAT ATT GT G GGT GAG ACT GAC GT-3′ (**Te50**); 5′-ACT TAC ACA CCT ACT ACT CCC TCA CTC AAT ATT GT G GGT GAG ACT GAC GT-3′ (**Te50Gclose**); and 5′-ACA ATA TTC ACT CAG CCA CTA CTA CCT CTG TAA CT-3′ (**Ta35**).

The 15mer base sequence used to capture the template is given in boldface; the underlined bases indicate those which serve as a template in the polymerase reaction. Ta35 is a synthetic oligonucleotide being complementary to the templating bases. The guanine bases, which can be paired with Cy5–dCTP during the DNA polymerization, are indicated in gray. Figure 2 shows a schematic presentation of the multilayer system described.

DNA extension assays were carried out using various concentrations of the exonuclease-free Klenow fragment of

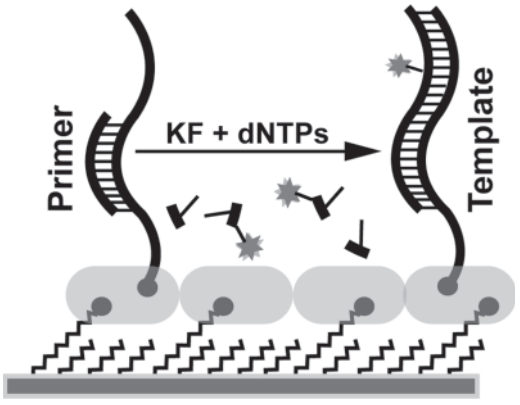

Figure 2. Schematic representation of the surface architecture.

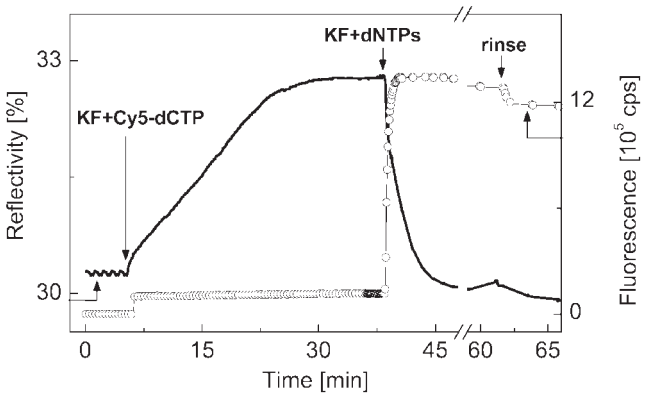

Figure 3. Example for a primer extension assay monitored by SPFS. First, KF (7.6 nM) was added together with Cy5–dCTP (1 μM). The extension process was not initiated at this point, since the first base on the template strand required the incorporation of dATP. The reflectivity increase after KF injection corresponds to the formation of a binary DNA–KF complex (solid line). Injection of the complete dNTP mixture (1 μM each) caused the release of KF and a rapid fluorescence increase (open circles) demonstrating the incorporation of Cy5-labeled nucleotides into surface-attached DNA. The refractive index change owing to the primer extension was below the sensitivity limit of SPR which is why the reflectivity returned to the initial value after the removal of the enzyme.

Escherichia coli DNA polymerase I (Amersham Pharmacia) in HSM buffer. The elongation was always initiated by the addition of a mixture of all four deoxynucleotidetriphosphates (dNTPs) and Cy5-labeled dCTP (both Amersham Pharmacia) at various concentrations.

Data acquisition and analysis

Since the evanescent field of the SP mode is sensitive to the optical environment, any adsorption of material to the gold layer will change the resonance angle. For non-absorbing layers, the shift in resonance angle is proportional to the product of the thickness gain, Δd, and change in refractive index, Δn: $\Delta\theta \propto \Delta n \cdot \Delta d$. Routinely, a SPR experiment starts with recording the changes of reflectivity as a function of the incidence angle (angle scan) for the blank gold surface immersed in running buffer. Kinetic measurements are carried out by monitoring the reflectivity as a function of time at a fixed angle of incidence. By definition, the angle chosen for kinetic measurements is the one corresponding to 30% reflectivity (at the low angle side of the resonance curve), which ensured that the reflectivity changed linearly with the resonance angle. After a new equilibrium is reached, a second angular reflectivity spectrum is monitored. Thickness parameters were then determined from Fresnel simulations of the scan curves acquired before and after the reaction of interest. Thickness parameters were converted into surface coverage using the following equation.

$$\Delta m_{\mathrm{SPR}} = d \cdot \frac{n_{\mathrm{film}} - n_{\mathrm{buffer}}}{\mathrm{d}n/\mathrm{d}c}, \qquad \mathbf{1}$$

with dn/dc being the refractive index increment in ml/g for the respective species bound.

RESULTS AND DISCUSSION

DNA immobilization and hybridization

The biosensor surface was composed as depicted in Figure 2. Because chromophors encounter significant quenching by the gold surface for dye-metal distances <5 nm (29,30), the reproducibility of a binding matrix that ensures a constant surface spacing and a constant number of DNA strands, is of great importance for obtaining comparable results from different gold chips. The possibility to follow on-line the build-up of each layer by SPR spectroscopy prior to the polymerase reaction provided maximum control over the layer composition. The surface spacing provided by the binding matrix was 1.5 nm for the thiol SAM and 4 nm for the streptavidin layer, which corresponds to a flat, monomolecular film (27,28). The thickness parameters for P45, Te50 and Ta35 (at n = 1.375) were found to be 2.8, 1.5 and 0.7 nm, respectively. The experimental variation was ±0.1 nm for streptavidin and ±0.25 nm for the various DNA films. According to the molar surface concentrations for streptavidin (3.5 pmol/cm^2) and P45 (4.7 pmol/cm^2), only 67% of the biotin-binding pockets harbored DNA strands (assuming two available biotin-binding sites per streptavidin molecule). This is reasoned by the electrostatic repulsion arising between two DNA strands bound in adjacent biotin-binding pockets given center-to-center distance of only 2.5 nm (31,32). Judging from the molar concentration determined for Te50 hybridization (2.3 pmol/cm^2), 48% of the primer strands were decorated with the Te50 and in turn, 50% of these duplexes hybridized to the Ta35 (1.6 pmol/cm^2). Causing a shift in reflectivity of only ~1%, the mass added upon hybridization of Ta35 was very close to the detection limit of the used SPR set-up, which suggests the use of an alternative enhancement mechanism to observe the DNA synthesis.

Primer extension assay

Figure 3 gives an example for an enzymatic primer extension assay monitored by SPFS in the kinetic mode. In this example, Cy5-labeled dCTP was incorporated at a single position of the synthesized DNA strand. After the attachment of the DNA substrate P45/Te50Gclose, a mixture of KF (7.6 nM) and Cy5–dCTP (1 μM) was exposed to the surface. The increase in reflectivity clearly demonstrates binding of the KF to DNA, while the background fluorescence, originating from bulk molecules staying within the range of the evanescent field, remains constant at ~1 × 10^5 c.p.s. DNA extension

was effectively inhibited in this situation as the first templating base required the incorporation of a nucleotide different from dCTP. At equilibrium, DNA extension was initiated by adding a mixture of KF (7.6 nM) and all four dNTPs (1 μM each, dCTP was fully substituted by the labeled analog). The system responded with a nearly instantaneous jump in fluorescence intensity and a decrease in the reflectivity to the initial value. These opposite effects were attributed to DNA growth due to the incorporation of dNTPs including the Cy5–dCTP and the simultaneous release of the enzyme from the completed double-stranded DNA. A spontaneous release of the enzyme after DNA synthesis has been observed in QCM studies previously (16). Rinsing with buffer confirmed the covalent linkage of the Cy5–dCTP.

Besides providing detailed insights into the polymerase/DNA interaction, this assay has potential as a method for DNA detection. In a two-step procedure, the analyte strands are first targeted by the immobilized probe and subsequently, the signal obtained for the hybridization event (originating from the refractive index change) is amplified by the fluorescent primer extension assay.

Variation of the label concentration

From the application-oriented point of view, it is important to know which label density yields the optimal sensitivity in the primer extension assay. Therefore, the number of Cy5-labels on the surface was varied by applying different mixing ratio of labeled and unlabeled dCTP (referred to as the mole fraction x_{Label}).

Since DNA polymerases have a high specificity for their natural substrates, the incorporation of the Cy5–dCTP is not expected to depend linearly on the mole fraction x_{Label}. Kinetic studies have established that base discrimination starts at the early stage of the reaction cycle as the correct nucleotide binds with much higher affinity to the binary polymerase/DNA complex than the incorrect one (33,34). It is generally believed that the binding of the correct nucleotide triggers the rate-limiting transition from the 'open' to the 'closed' ternary complex (35–37), which is the catalytically competent species. The closed complex contains a binding pocket that snuggly surrounds the nascent base pair and aligns the catalytic center. In aqueous solution the contribution of proper base–base hydrogen bonding is only 0.2–4 kcal/mol (38). It has been proposed that the enzyme amplifies the energy differences by excluding water from the active site, thus increasing enthalpy and reducing entropy differences. More dominantly, the selectivity depends on the base pair geometry. While the geometries of AT and GC base pairs are remarkably similar to each other, they differ largely from those of mismatched base pairs (33,34,38). For instance, non-polar bases that mimic the size and the shape of normal bases but are incapable of Watson–Crick base pairing can be incorporated with high selectivity (38,39).

In the used Cy5–dCTP, the dye was attached to the C5 of the nucleobase via a methylene linker. While the attachment of a dye at this position does not interfere with Watson–Crick base pairing, it changes the geometry of the labeled base pair, even if long alkyl chains are used as linkers between dye and dNTP. Figure 4a shows SPFS scan curves obtained after the extension of the duplex P45/Te50Gclose at mole fractions $x_{\mathrm{Label}} = 1$, 0.9, 0.75, 0.5 and 0.25, respectively (at [KF] = 7.6 nM and $[\mathrm{dNTP}]_{\mathrm{total}}$ = 1 μM). A DNA template containing a single guanine base was used to reduce the complexity of the reaction to a single incorporation event. While the SPR scan curves were identical in shape (only one example is shown), the height of the fluorescence scan curves increased with increasing x_{Label}. Plotting the peak fluorescence values versus x_{Label} revealed a sublinear increase (Figure 4b). Accordingly, the incorporation of labeled dCTP is not a statistical process; however, it highly favors the natural substrate. This result is in good agreement with the previous results addressing the label efficiency in dependence of the chemical nature of the attached dye, the linker moiety used for attachment of the dNTP and the nucleobase to which the dye was attached

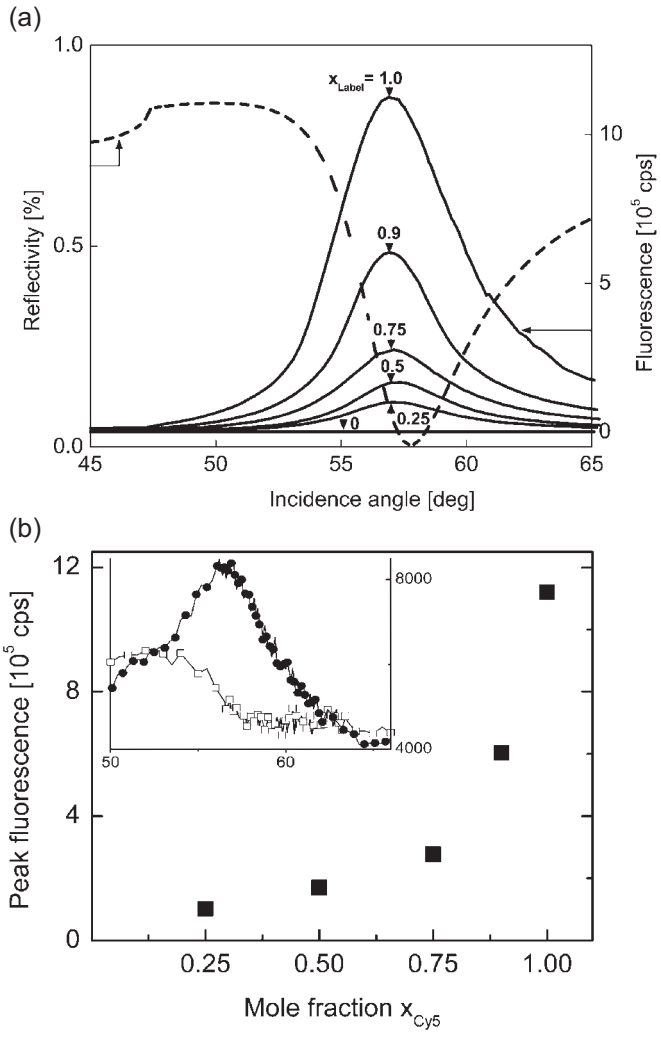

Figure 4(a). SPFS scan curves recorded after the elongation of P45/Te50G1close using different mole fractions of Cy5–dCTP, x_{Label}. The total dNTP concentration was 1 μM and KF was bound to DNA from a 7.6 nM solution before the addition of dNTP. One exemplary reflectivity curve is shown as a dotted line; the fluorescence curves are given as straight lines and marked with the corresponding mole fractions. (**b**) Plot of the final fluorescence values versus x_{Label} according to the raw data shown on top. The plot is not linear revealing the non-stochastic nature of the label incorporation. The inset shows the SPFS scan curve monitored after primer extension at a mole fraction $x_{\mathrm{Label}} = 0.001$. The yielded fluorescence intensity corresponds to a label density of 6 Cy5-molecules per μm^2.

(40–42). Utilizing PCR, random priming or nick translation as labeling techniques, these studies agreed in that it was hardly possible to achieve quantitative substitution of a nucleotide by its labeled analog in long DNA fragments that require frequent additions of the labeled nucleotide. Instead, an inverse relationship was found between modified DNA product yield and the content of incorporated dye-dNTPs. Thus, the number of chain termination events increased with an increasing number of dye labels present in the primer strand. In addition, modifications of the template strand were reported to be less inhibitive than those of the primer strand although they interfere with primer hybridization in PCRs, which also provokes reduced yields. The design of our experiments is different in that it examined the incorporation of dNTPs at a single site of the DNA strand. Consequently, processes that are relevant in PCRs such as primer hybridization after duplex melting or rebinding of the enzyme to heavily labeled DNA regions did not play a role. Hence, our result demonstrates that the discrimination between labeled and unlabeled dNTP substrates occurs during the early stage of nucleotide selection and the reduced labeling yield is not entirely a consequence of perturbed interactions between the DNA polymerase and the already labeled primer/template duplex. The rapid increase in the curve (Figure 4b) suggests the use of $x_{\text{Label}} \geqslant 0.5$ for kinetic studies employing this DNA construct. This will substantially improve the signal-to-noise level since the relative background fluorescence caused by unattached chromophors in the bulk will be lower.

The described experiments are suited to estimate the detection limit for incorporated Cy5–dCTP. Utilizing a mole fraction of $x_{\text{Label}} = 0.001$ in the elongation reaction still resulted in a fluorescence yield of ~8500 c.p.s. The inset in Figure 4b displays the corresponding fluorescence scan curves before and after the primer extension. Note that the data plotted in the main graph were recorded through a 1.3 dB gray filter that attenuated the signal by a factor of 19 (as determined experimentally). If we assume that 100% of the available DNA duplexes (2.3 pmol/cm^2) were labeled at $x_{\text{Label}} = 1$, a fluorescence intensity of 8500 c.p.s. corresponds to 0.04% labeled DNA strands. Hence, the use of SPFS enabled us to detect a label concentration of ~900 amol/cm^2, which equals ~6 Cy5-molecules per μm^2. This result is in good agreement with the sensitivity recently determined for the detection of antibodies by SPFS (21).

To test whether the detection limit can be further improved by multilabeling of the template strands, duplex P45/Te50 (containing 12 randomly distributed guanines) was extended at different mole fractions x_{Label}. For mole fractions >0.1, intramolecular quenching effects were observed that showed evidence of a rapid increase in the fluorescence intensity during the initial phase of the reaction followed by a subsequent drop if the reaction proceeded (data not shown). Using $x_{\text{Label}} = 0.1$, the final fluorescence intensity observed was maximal and equaled the intensity measured for the extension of P45/Te50Gclose at $x_{\text{Label}} = 1$. The conclusion is that the detection limit for captured DNA of this length cannot be improved further by multilabeling of the DNA strands because every additional dye-molecule causes intramolecular quenching effects. The situation might be different for templates of lower guanine content or longer templates and should be studied more systematically.

Effect of DNA polymerase concentration

In order to test whether the enzyme molecules bound to the surface-attached DNA retain their catalytic activity, the velocity of DNA synthesis was assessed as a function of the amount of immobilized KF. Note that in the primer extension kinetic presented above (Figure 3), the extension reaction was initiated by the addition of a mixture of KF and dNTPs to make sure that the dissociation of the enzyme was not caused by the adjustment of a new binding equilibrium owing to the exchange of solutions. In the present experiments, only dNTPs were added in this step forcing the already bound molecules to action.

Identical surfaces were prepared by anchoring prehybridized P45/Te50 (1 μM) on the streptavidin layer. These surfaces were exposed to KF at solution concentrations ranging from 1.5 to 30 nM and primer extension was initiated by the addition of a 10 μM solution of dNTP ($x_{\text{Label}} = 0.025$). For a clearer presentation, SPR and fluorescence curves are displayed in separate figures (Figure 5a and b, respectively). The amount of DNA-bound KF raised with increasing solution concentrations. The equilibrium reflectivity data were translated into surface concentrations using Equation 1 ($n_{\text{KF}} = 1.45$, dn/dc = 0.212 ml/g) and plotted against the corresponding solution concentrations (Figure 5c). Fitting the data using a 1:1 binding model yielded the affinity constant as $K_A = 1.5 \times 10^8$ M^{-1}. The value compares fairly well with those obtained from solution methods. Depending on the method and the DNA constructs that were used the published values vary between 2×10^8 and 20×10^8 M^{-1} (43–46). The maximum surface load of 108 ng/cm^2 (1.7 pmol/cm^2) reveals that 46% of the streptavidin molecules exhibit a binary polymerase–DNA complex. This amount corresponds to the number of double-stranded DNA substrates available on the surface.

The injection of the dNTP solution caused a rapid increase in the fluorescence intensity accompanied by a decrease in the reflectivity. As shown in Figure 5d, the initial slopes of the fluorescence signal increased linearly with increasing KF surface coverage clearly demonstrating that the bound KF is the catalytically active species. The decrease in the reflectivity curve reflects the dissociation of the enzyme from the completely double-stranded DNA and can be described as follows:

$$\text{DNA}_{\text{extended}}/\text{KF} \underset{k_{\text{off}}}{\overset{k_{\text{on}}}{\rightleftharpoons}} \text{DNA}_{\text{extended}} + \text{KF}$$

$$-[\text{DNA}/\text{KF}]_t = -[\text{DNA}/\text{KF}]_\infty[1 - \exp(-t/\tau)]$$

$$\tau^{-1} = k_{\text{on}}[\text{KF}] + k_{\text{off}}. \qquad \mathbf{2}$$

The linear presentation of τ^{-1} versus [KF] yielded $k_{\text{off}} = 0.007$ s^{-1} and $k_{\text{on}} = 2.6 \times 10^5$ M^{-1} s^{-1} (Figure 5e). Thus, K_A decreased from 1.5×10^8 to 3.7×10^7 M^{-1} after the elongation reaction. It is not fully understood why the reflectivity curves did not return to the baseline before rinsing with buffer (data not shown) when the experiments were carried out at KF concentrations >33 ng/cm^2. The rinsing step caused a second single exponential decay whose rate decreased linearly with concentration. Rates of 1.9×10^{-3}, 2.8×10^{-3} and 4×10^{-3} s^{-1} were found at 80, 92 and 108 ng/cm^2 surface coverage, respectively. If the second decay rates were equal, one would assume that the remaining mass

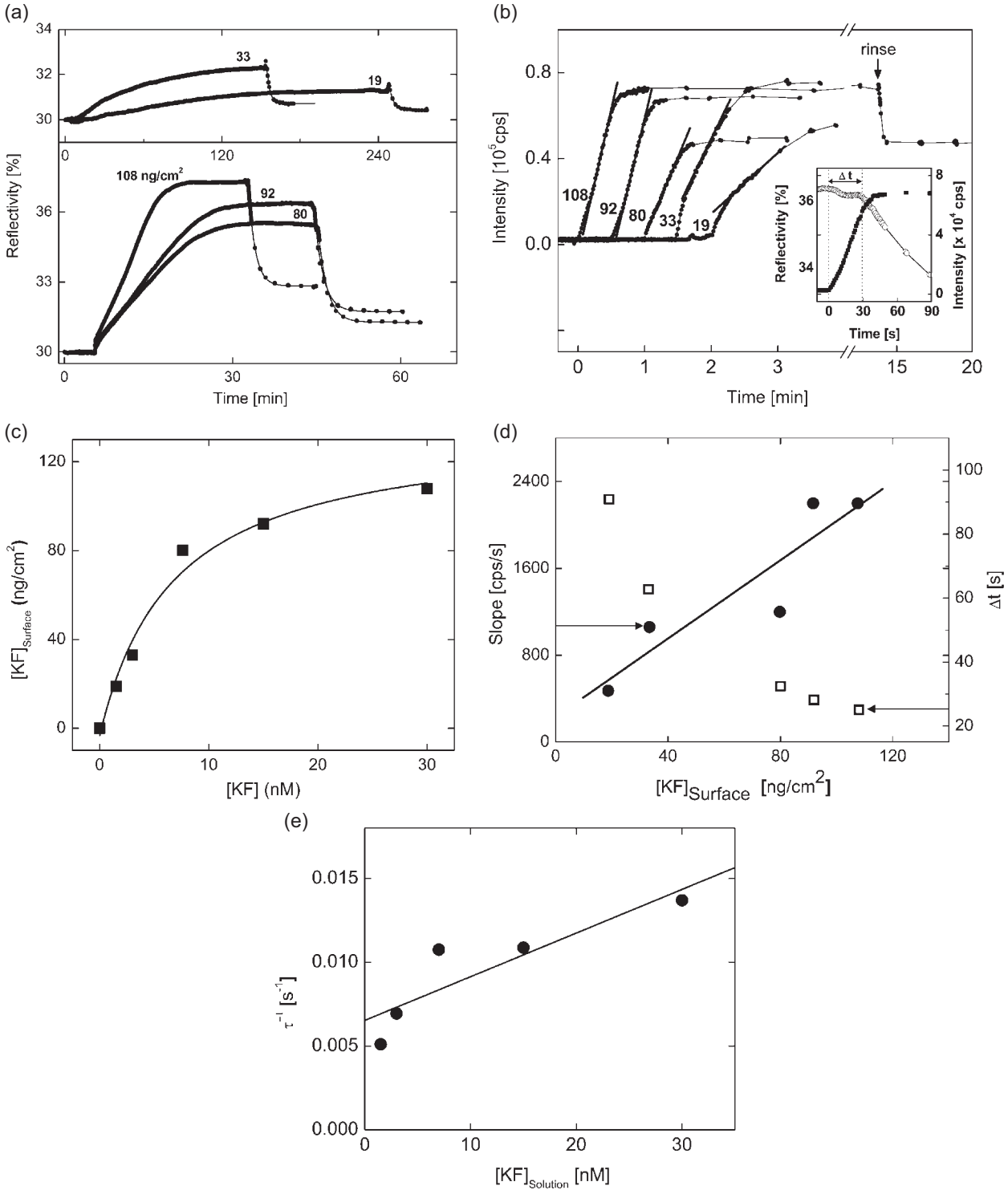

Figure 5. Influence of the amount of bound KF on the velocity of DNA replication and KF release. Shown are five sets of experiments that were carried out with varying bulk concentrations of KF (between 1.5 and 30 nM). DNA synthesis was initiated by the addition of identical amounts of dNTPs (10 μM each with $x_{Cy5} = 0.025$). (**a**) Time evolution of the reflectivity (solid dots). The exponential decay of the curves after dNTP addition was fitted using Equation 2 (solid lines). Owing to different time courses, curves corresponding to very low KF concentrations are shown in a separate panel (top). (**b**) Fluorescence curves monitored simultaneously with the reflectivity curves shown in (a). The time of dNTP injection is offset to zero and the curves are shifted relative to each other for a clearer presentation. The inset explains the temporal connection between the fluorescence and the reflectivity data. (**c**) Affinity of the KF to recessed DNA duplexes. Plotting the immobilized amount of KF according to (a) versus the corresponding solution concentration (closed squares) yields $K_A = 1.5 \times 10^8\ M^{-1}$ using a 1:1 binding model (solid line). (**d**) Plot of the initial slopes of the fluorescence curves as displayed in (b) versus surface concentration of KF (closed circles). The primer extension rate was found to depend linearly on the amount of bound KF. Also plot of Δt, which is the time that elapses between the start of the fluorescence rise and that of the reflectivity decay, versus KF concentration (open squares). (**e**) Change of binding affinity after complete primer extension. Plotting τ^{-1} versus [KF] produced a linear curve that determines the affinity constant to be $K_A = 3.7 \times 10^7\ M^{-1}$.

corresponds to KF bound to complete double strands as the affinity decreases only by one order of magnitude in the course of the primer extension reaction. In contrast, the measured second k_{off} rates are smaller than the first k_{off} rates inferring a higher affinity. This result suggests the existence of non-extended DNA strands. However, it does not appear logical that high-KF concentrations promote more incomplete DNA synthesis.

As explained in the inset of Figure 5b, different KF concentrations also cause differences in the response of the SPR and the fluorescence curve relative to each other. The higher the KF concentration the smaller is the time delay between the start of the fluorescence increase and that of the reflectivity decrease. Figure 5d displays the time delay, Δt, as a function of KF concentration. The fluorescence slopes depend linearly on the KF concentration, whereas the time delay shows a sublinear dependency at high-KF concentration. This result argues for a prompt insertion of the labeled nucleotide at the beginning of the template strand, whereas a further rate-limiting step must occur at a later stage of the reaction. As the reflectivity remains unaffected during this delay time, the complete release of the KF from the immature strands appears unlikely, but pausing of the process could be possible given the low processivity of the KF.

Effect of dNTP concentration

The Michaelis–Menten approach is a simple kinetic model suited for the description of the DNA extension process. In this model, the immobilized KF–DNA complex is considered to be the catalytically active species with the dNTPs as the substrates becoming covalently linked to the nascent DNA strand in the course of the reaction.

$$(\mathrm{KF/DNA}_n)_{\mathrm{im.}} + \mathrm{dNTP} \underset{k_1}{\overset{k_{-1}}{\rightleftharpoons}} (\mathrm{KF/DNA}_n/\mathrm{dNTP})_{\mathrm{im.}} \overset{k_{\mathrm{cat}}}{\rightarrow} (\mathrm{KF/DNA}_{n+1})_{\mathrm{im.}} + \mathrm{P_2O_7^{-4}},$$

where n denotes the number of nucleotides in the DNA strand. The initial velocity of nucleotide incorporation, V_i, depends on the substrate concentration as follows:

$$V_i = \frac{k_{\mathrm{cat}}[\mathrm{KF/DNA}_n]_0[\mathrm{dNTP}]}{K_M + [\mathrm{dNTP}]} \quad \text{with } K_M = \frac{k_{\mathrm{cat}} + k_{-1}}{k_1}. \qquad \mathbf{3}$$

The common method to determine the catalytic constants according to this model is to measure the initial reaction velocities as a function of the dNTP concentration. In the particular case of SPFS, the chosen concentration range was governed by two limiting factors: high Cy5–dCTP concentration gave rise to a high background fluorescence caused by bulk molecules excited within the evanescent field at the interface. In principle, dilution of Cy5–dCTP with unmodified dCTP and using Cy5–dCTP only as an indicator would be effective in reducing the background fluorescence. However, since the KF strongly prefers the natural substrate, a mole fraction $x_{\mathrm{Label}} \geqslant 0.5$ must be applied to achieve satisfying dye incorporation. Here, the extension of the P45/Te50Gclose duplex was carried out by employing a fixed KF concentration (7.6 nM) and varying the dNTP concentrations between 5 and 2000 nM ($x_{\mathrm{Label}} = 0.5$). By using the P45/Te50Gclose substrate, the reaction observed was limited to a single incorporation event at the beginning of the polymerization reaction. In all experiments the KF immobilization caused a uniform reflectivity shift of ~4%; this step is not presented here. Figure 6a and b summarizes the SPR and fluorescence curves, respectively, starting at the time of dNTP addition. The reduction in the dNTP concentration had the following effects: first, the final values of fluorescence were decreased indicating a reduced number of incorporated Cy5–dNTP molecules. Second, the decrease in the fluorescence slopes corresponded to a deceleration of the polymerization reaction, which is also reflected in lower time constants for the single exponential decrease of the SPR signal. While the SPR signal returned to the baseline in the presence of high-dNTP concentrations, the total reflectivity decrease was smaller at lower concentrations. Complete release of the enzyme could be triggered by injecting a large amount of dNTPs at this point (data not shown). This finding indicates that some KF molecules remained bound to incomplete, still recessed 3′ termini. K_M was calculated from the linear Lineweaver–Burk presentation, plotting V_i^{-1} versus $c(\mathrm{dNTP})^{-1}$ (Figure 6c). The values corresponding to 5 and 50 nM dNTPs were omitted because a pre-requisite for using the Michaelis–Menten kinetics is the excess of substrate over the enzyme concentration, which is not fulfilled under these conditions. K_M for the incorporation of Cy5–dCTP was found to be 3.4 μM, which compares well with literature values for the incorporation of unlabeled dNTPs. These were reported to be 7 μM for dTTP, 5 μM for dGTP incorporation and 1.3–3.1 μM for mixed sequences (44,45).

Influence of base mismatches

DNA polymerases have the ability to copy DNA with extremely high fidelity; for DNA polymerase I, the probability of an error during replication is $<10^{-6}$ per nucleotide addition (47). The mechanisms available to reduce the error rate are (i) selection of the correct dNTP, (ii) inefficient extension of mispaired 3′ primer termini and (iii) excision of the mispaired base from the primer terminus by the proofreading 3′–5′ exonuclease activity (48). In the crystal structure of the KF the polymerase and exonuclease active sites are spatially separated by 30 Å (49). While DNA was shown to bind as double strand at the polymerase site, the exonuclease domain strongly favors single-stranded DNA. Upon proofreading, the primer terminus must shuttle from one active site to the other. For KF two pathways are reported: the intermolecular pathway postulates dissociation of the polymerase–DNA complex and subsequent rebinding at the exonuclease site. Alternatively, the primer terminus translocates intramolecularly from the polymerase to the exonuclease domain by melting 3–4 bp at the primer terminus (50). Fluorescence anisotropy measurements using dansyl-labeled DNA substrates exhibiting terminal, internal or consecutive mismatches within the last four bases of the primer terminus revealed substantially increased partitioning constants K_{pe} (giving the ratio of DNA bound to the exonuclease and KF bound to the polymerase domain) (50). These results demonstrate that proofreading is not a randomly occurring process but it is triggered by aberrations in the geometry and melting capacity of the primer terminus. Although this intramolecular pathway for traveling between the exonuclease and the polymerase site is available to the enzyme, it is not invariably used; in any case, the

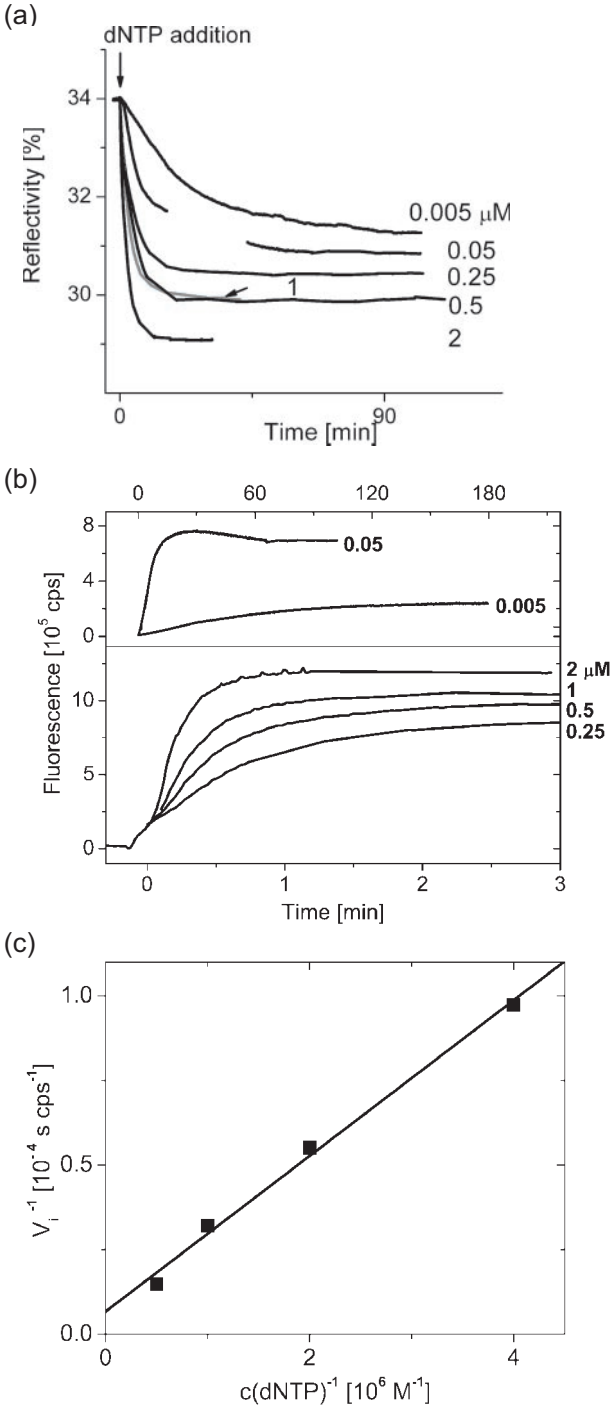

Figure 6. Replication rates as a function of total dNTP concentration. x_{Label} was 0.5 and identical surface concentration of KF were applied (80 ng/cm^2). (**a**) Time courses of the reflectivity starting from the time of dNTP injection. (**b**) The fluorescence slopes were proportional to the dNTP substrate concentration. (**c**) Lineweaver–Burk plot yielding K_M = 3.4 µM.

dissociation rate will increase upon introduction of a mismatch to the primer terminus causing lower affinities to these substrates.

In this paragraph, the influence of two types of base mismatches in the primer/template region on DNA binding and elongation will be demonstrated: the P45/Te50tmm substrate

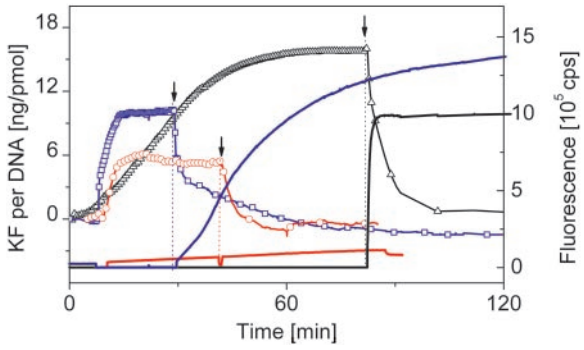

Figure 7. Influence of single base mismatches in the primer/template region on the primer extension and the KF binding. While the internal mismatch 3 nt upstream the 3′-terminus of the primer decelerated the elongation process (blue), a terminal mismatch inhibited the reaction entirely (red). The extension of the fully matched primer carried out at identical conditions is shown in black.

carried a terminal G–G mismatch while the P45/Te50imm substrate exhibited a G–G mismatch 3 nt upstream of the 3′ terminus of the primer. The stability of the two different DNA substrates has been checked using SPR. While the immobilization of the three different primers differing only in a single base caused identical reflectivity shifts (corresponding to a surface coverage of ~65 ng/cm^2), the reflectivity shift observed for the formation of the fully complementary duplex (37 ng/cm^2) was almost twice as high as that found for the singly mismatched duplexes (21 ng/cm^2). Thus, in experiments probing the KF binding to mismatched DNA substrates, only half the number of binding sites was available.

Figure 7 compares the enzymatic extension of DNA substrates being either fully complementary or singly mismatched, carried out at otherwise identical conditions: 7.6 nm KF were immobilized before the addition of 0.5 µM dATP, dGTP, dTTP and Cy5–dCTP. In the presented plots, the reflectivity has been converted into mass per mole of immobilized DNA. While ~16 ng/pmol KF bound to the perfectly matched DNA substrate, only 10 and 5 ng/pmol KF were observed for the DNA substrates having an internal and a terminal mismatch, respectively.

However, the association rate of binding to mismatched DNA seemed to be faster than that for the matching DNA substrate and lacked the initial linear binding phase. Addition of dNTP substrates did not initiate DNA polymerization in the presence of a terminal mismatch, although it caused the enzyme's release. The replication process was tremendously slowed down for the P45/Te50imm substrate; it finished after 80 min compared with 3 min for P45/Te50. In the case of P45G/Te50imm, the majority of the enzyme molecules were released prior to completeness of the polymerization reaction, which could indicate a lower processivity caused by translocation between the exonuclease and the polymerase domain via the intermolecular pathway. Thus, the reaction is often interrupted by dissociation and rebinding events. Carver *et al*. (50) used similar primer/template duplexes, also having three terminal cytosines, in time-resolved fluorescence studies and found partitioning coefficients K_{pe} of 0.22 for terminal G–G mismatches and 0.46 for an internal G–G mismatch 3 nt upstream of the 3′-primer terminus (cf. K_{pe} = 0.07 for

fully complementary oligonucleotides) (Figure 7). Thus, the internal mismatch had a stronger impact on K_{pe} than the terminal one, which explains the faster dissociation from P45G/Te50imm.

CONCLUSIONS

We have presented a broad SPFS study of enzymatic primer extension that demonstrates the merit of the technique for two objectives: these are the sensitive detection of DNA and studies of the dynamics of enzyme–DNA interaction.

Dye-labeled nucleotides, which were incorporated into surface-tethered DNA by a polymerase reaction, were detected at subfemtomolar concentration. The incorporation was proven to be highly base sensitive, hence enabling the detection of single point mutations either by inhibition or by deceleration of the reaction rate depending on the position of the base mismatch. Indeed, enzymatic DNA synthesis has been followed by SPR spectroscopy alone, but by far not with the sensitivity reported here.

The binding and catalytic constants for the interaction of the Klenow fragment with DNA were measured by SPFS and found to be in good agreement with those obtained from conventional solution methods. The strength of SPFS is that KF binding and nucleotide incorporation are attributed to different physical measures, the reflectivity and the fluorescence intensity, which separates the response for enzyme binding from that of enzyme activity. In conventional SPR spectroscopy, the mass loss during enzyme release counteracts the mass increase owing to DNA extension making it difficult to retrieve reaction rates. An interesting application of the extension assay would be the rapid screening of binding and catalytic activity of different protein mutants whose amino acids have been altered by mutagenesis, which elucidates the role of certain amino acids. Using SPFS, one could immediately tell whether the fluorescence yield was lowered because of changes in the binding affinity, the instability of the DNA duplex or catalytic inhibition of the enzyme. Numerous biological reactions involving cleavage, ligation or synthesis of oligonucleotides could be designed in a way that is compatible with the described biosensor scheme.

Comparable sensitivities for fluorescence detection can only be achieved by single molecule-sensitive techniques, such as fluorescence correlation spectroscopy (FCS) and fluorescence microscopy either in TIR or in confocal geometry (51). FCS reports diffusion coefficients and concentration but has the limitation that it is only useful in kinetic studies of systems that substantially change their hydrodynamic radius in the course of the reaction (52). To overcome this limitation, dual color FCS was established (53). For instance, DNA hybridization can be visualized by the attachment of two different labels at both strands, which are excited and detected by independent lasers and photon counters, respectively. This method has been proven to be efficient in many kinetic studies (54). TIRF microscopy offers the possibility to observe several single molecules in parallel but its merit for fast kinetics is limited by the time-resolution of the CCD camera. An even better surface confinement than TIRF is offered by SAF (55,56). A glass–water interface is illuminated from below through the glass with a focused laser beam. A parabolic lens collects the SAF signal, which is the fluorescence emitted into the angular region above the critical angle of refraction. In principle, SAF provides the same fluorescence information as SPFS does, but it lacks the possibility to monitor the immobilization of unlabeled surface compounds. The surface control provided through the reflectivity in SPFS facilitates the optimization of the assay conditions (for instance fine-tuning of the DNA probe density) and reduces the risk of misinterpretation owing to irreproducible surface functionalization. In summary, SPFS method is a real-time method that is extremely sensitive without the requirement of *ex situ* labeling of the involved oligonucleotides, it provides the convenience of a biosensor format and works with instrumentation that is relatively inexpensive compared with single molecule fluorescence microscopes.

ACKNOWLEDGEMENTS

Funding to pay the Open Access publication charges for this article was provided by EU grant (DNA track, QLKI-2000-01658).

Conflict of interest statement. None declared.

REFERENCES

1. Makrigiorgos,G.M. (2004) PCR-based detection of minority point mutations. *Hum. Mutat.*, **23**, 406–412.
2. Kwok,P.Y. (2001) Methods for genotyping single nucleotide polymorphisms. *Annu. Rev. Genom. Hum. Genet*, **2**, 235–258.
3. Sanger,F., Nicklen,S. and Coulson,A.R. (1977) DNA sequencing with chain-terminating inhibitors. *Proc. Natl Acad. Sci. USA*, **74**, 5463–5467.
4. Hyman,E.D. (1988) A new method of sequencing DNA. *Anal. Biochem.*, **174**, 423–436.
5. Franca,T.C., Carrilho,E. and Kist,T.B.L. (2002) A review of DNA sequencing techniques. *Q. Rev. Biophys.*, **35**, 169–200.
6. Samiotaki,M., Kwiatkowski,M., Parik,J. and Landegren,U. (1994) Dual-color detection of DNA-sequence variants by ligase-mediated analysis. *Genomics*, **20**, 238–242.
7. Komiyama,M., Ye,S., Liang,X.G., Yamamoto,Y., Tomita,T., Zhou,J.M. and Aburatani,H. (2003) PNA for one-base differentiating protection of DNA from nuclease and its use for SNPs detection. *J. Am. Chem. Soc.*, **125**, 3758–3762.
8. Lyamichev,V., Mast,A.L., Hall,J.G., Prudent,J.R., Kaiser,M.W., Takova,T., Kwiatkowski,R.W., Sander,T.J., de Arruda,M., Arco,D.A., Neri,B.P. and Brow,M.A.D. (1999) Polymorphism identification and quantitative detection of genomic DNA by invasive cleavage of oligonucleotide probes. *Nat. Biotechnol.*, **17**, 292–296.
9. Pastinen,T., Raitio,M., Lindroos,K., Tainola,P., Peltonen,L. and Syvanen,A.C. (2000) A system for specific, high-throughput genotyping by allele-specific primer extension on microarrays. *Genome Res.*, **10**, 1031–1042.
10. Schweitzer,B. and Kingsmore,S. (2001) Combining nucleic acid amplification and detection. *Curr. Opin. Biotechnol.*, **12**, 21–27.
11. Tsoi,P.Y. and Yang,M. (2002) Kinetic study of various binding modes between human DNA polymerase beta and different DNA substrates by surface-plasmon-resonance biosensor. *Biochem. J.*, **361**, 317–325.
12. Okumoto,Y., Tanabe,Y. and Sugimoto,N. (2003) Factors that contribute to efficient catalytic activity of a small Ca^{2+}-dependent deoxyribozyme in relation to its RNA cleavage function. *Biochemistry*, **42**, 2158–2165.
13. Pemberton,I.A. and Buckle,M. (1999) Real time *in vitro* analysis of transcription by RNA polymerase on immobilized DNA fibres. *J. Mol. Recognit.*, **12**, 322–327.
14. Buckle,M., Williams,R.M., Negroni,M. and Buc,H. (1996) Real time measurements of elongation by a reverse transcriptase using surface plasmon resonance. *Proc. Natl Acad. Sci. USA*, **93**, 889–894.
15. Delagoutte,E. and Hippel,P.H. (2003) Function and assembly of the bacteriophage T4 DNA replication complex. *J. Biol. Chem.*, **278**, 25435–25447.

16. Matsuno,H., Niikura,K. and Okahata,Y. (2001) Direct monitoring kinetic studies of DNA polymerase reactions on a DNA-immobilized quartz-crystal microbalance. *Chem. Eur. J.*, **7**, 3305–3312.
17. Liebermann,T. and Knoll,W. (2000) Surface-plasmon field-enhanced fluorescence spectroscopy. *Colloid Surface A*, **171**, 115–130.
18. Liebermann,T., Knoll,W., Sluka,P. and Herrmann,R. (2000) Complement hybridization from solution to surface-attached probe-oligonucleotides observed by surface-plasmon-field-enhanced fluorescence spectroscopy. *Colloid Surface A*, **169**, 337–350.
19. Tawa,K. and Knoll,W. (2004) Mismatching base-pair dependence of the kinetics of DNA–DNA hybridization studied by surface plasmon fluorescence spectroscopy. *Nucleic Acids Res.*, **32**, 2372–2377.
20. Yu,F., Yao,D.F. and Knoll,W. (2003) Surface plasmon field-enhanced fluorescence spectroscopy studies of the interaction between an antibody and its surface-coupled antigen. *Anal. Chem.*, **75**, 2610–2617.
21. Yu,F., Persson,B., Lofas,S. and Knoll,W. (2004) Attomolar sensitivity in bioassays based on surface plasmon fluorescence spectroscopy. *J. Am. Chem. Soc.*, **126**, 8902–8903.
22. Krieg,A., Laib,S., Ruckstuhl,T. and Seeger,S. (2003) Real-time detection of nucleotide incorporation during complementary DNA strand synthesis. *ChemBioChem*, **4**, 589–592.
23. Krieg,A., Laib,S., Ruckstuhl,T. and Seeger,S. (2004) Fast detection of single nucleotide polymorphisms (SNPs) by primer elongation with monitoring of supercritical-angle fluorescence. *ChemBioChem*, **5**, 1680–1685.
24. Schmidt,P.M., Lehmann,C., Matthes,E. and Bier,F. (2002) Detection of activity of telomerase in tumor cells using fiber optical biosensors. *Biosens. Bioelectron.*, **17**, 1081–1087.
25. Levene,M.J., Korlach,J., Turner,S.W., Foquet,M., Craighead,H.G. and Webb,W.W. (2003) Zero-mode waveguides for single-molecule analysis at high concentrations. *Science*, **299**, 682–685.
26. Braslavsky,I., Hebert,B., Kartalov,E. and Quake,S.R. (2003) Sequence information can be obtained from single DNA molecules. *Proc. Natl Acad. Sci. USA*, **100**, 3960–3964.
27. Knoll,W., Zizlsperger,M., Liebermann,T., Arnold,S., Badia,A., Liley,M., Piscevic,D., Schmitt,F.J. and Spinke,J. (2000) Streptavidin arrays as supramolecular architectures in surface-plasmon optical sensor formats. *Colloid Surface A*, **161**, 115–137.
28. Häussling,L., Ringsdorf,H., Schmitt,F.-J. and Knoll,W. (1991) Biotin-functionalized self-assembled monolayers on gold-surface plasmon optical studies of specific recognition reactions. *Langmuir*, **7**, 1837–1840.
29. Vasilev,K., Knoll,W. and Kreiter,M. (2004) Fluorescence intensities of chromophores in front of a thin metal film. *J. Chem. Phys.*, **120**, 3439–3445.
30. Malicka,J., Gryczynski,Z. and Lakowicz,J.R. (2003) Effects of fluorophore-to-silver distance on the emission of cyanine-dye-labeled oligonucleotides. *Anal. Biochem.*, **315**, 57–66.
31. Weber,P.C., Ohlendorf,D.H., Wendoloski,J.J. and Salemme,F.R. (1989) Structural origins of high-affinity biotin binding to streptavidin. *Science*, **243**, 85–88.
32. Darst,S.A., Ahlers,M., Meller,P.H., Kubalek,E.W., Blankenburg,R., Ribi,H.O., Ringsdorf,H. and Kornberg,R.D. (1991) Two-dimensional crystals of streptavidin on biotinylated lipid layers and their interactions with biotinylated macromolecules. *Biophys. J.*, **59**, 387–396.
33. Kunkel,T.A. and Bebenek,K. (2000) DNA replication fidelity. *Ann. Rev. Biochem.*, **69**, 497–529.
34. Beard,W.A. and Wilson,S.H. (2003) Structural insights into the origins of DNA polymerase fidelity. *Structure*, **11**, 489–496.
35. Joyce,C.M. and Benkovic,S.J. (2004) DNA polymerase fidelity: kinetics, structure, and checkpoints. *Biochemistry*, **43**, 14317–14324.
36. Doublie,S., Sawaya,M.R. and Ellenberger,T. (1999) An open and closed case for all polymerases. *Structure*, **7**, R31–R35.
37. Li,Y., Korolev,S. and Waksman,G. (1998) Crystal structures of open and closed forms of binary and ternary complexes of the large fragment of *Thermus aquaticus* DNA polymerase I: structural basis for nucleotide incorporation. *EMBO J.*, **17**, 7514–7525.
38. Kool,E.T. (2002) Active site tightness and substrate fit in DNA replication. *Annu. Rev. Biochem.*, **71**, 191–219.
39. Kool,E.T. (1998) Replication of non-hydrogen bonded bases by DNA polymerases: a mechanism for steric matching. *Biopolymers*, **48**, 3–17.
40. Tasara,T., Angerer,B., Damond,M., Winter,H., Dörhöfer,S., Hubscher,U. and Amacker,M. (2003) Incorporation of reporter molecule-labeled nucleotides by DNA polymerases. II. High-density labeling of natural DNA. *Nucleic Acid Res.*, **31**, 2636–2646.
41. Zhu,Z. and Waggoner,A.S. (1997) Molecular mechanism controlling the incorporation of fluorescent nucleotides into DNA by PCR. *Cytometry*, **28**, 206–211.
42. Yu,H., Chao,J., Patek,D., Mujumdar,R., Mujumdar,S. and Waggoner,A.S. (1994) Cyanine dye dUTP analogues for enzymatic labeling of DNA probes. *Nucleic Acids Res.*, **22**, 3226–3232.
43. Bailey,M.F., van der Schans,E.J.C. and Millar,D. (2004) Thermodynamic dissection of the polymerizing and editing modes of a DNA polymerase. *J. Mol. Biol.*, **336**, 673–693.
44. Kuchta,R.D., Benkovic,P. and Benkovic,S.J. (1988) Kinetic mechanism whereby DNA-Polymerase I (Klenow) replicates DNA with high fidelity. *Biochemistry*, **27**, 6716–6725.
45. Gangurde,R. and Modak,M.J. (2002) Participation of active-site carboxylates of *Escherichia coli* DNA polymerase I (Klenow fragment) in the formation of a prepolymerase ternary complex. *Biochemistry*, **41**, 14552–14559.
46. Dahlberg,M.E. and Benkovic,S.J. (1991) Kinetic mechanism of DNA–polymerase-I (Klenow fragment)—identification of a second conformational change and evaluation of the internal equilibrium constant. *Biochemistry*, **30**, 4835–4843.
47. Loeb,L.A. and Kunkel,T.A. (1982) Fidelity of DNA synthesis. *Annu. Rev. Biochem.*, **51**, 429–457.
48. Bebenek,K., Joyce,C.M., Fitzgerald,M.P. and Kunkel,T.A. (1990) The fidelity of DNA-synthesis catalyzed by derivatives of *Escherischia coli* DNA–polymerase I. *J. Biol. Chem.*, **265**, 13878–13887.
49. Freemont,P.S., Friedman,J.M., Beese,L.S., Sanderson,M.R. and Steitz,T.A. (1988) Cocrystal structure of an editing complex of Klenow fragment with DNA. *Proc. Natl Acad. Sci. USA*, **85**, 8924–8928.
50. Carver,H.R., Hochstrasser,R.A. and Millar,D.P. (1994) Proofreading DNA-recognition of aberrant DNA termini by the Klenow fragment of DNA polymerase I. *Proc. Natl Acad. Sci. USA*, **91**, 10670–10674.
51. Haustein,E. and Schwille,P. (2004) Single-molecule spectroscopic methods. *Curr. Opin. Struct. Biol.*, **14**, 531–540.
52. Eigen,M. and Rigler,R. (1994) Sorting single molecules—application to diagnostics and evolutionary biotechnology. *Proc. Natl Acad. Sci. USA*, **91**, 5740–5747.
53. Schwille,P., Meyer-Almes,F.J. and Rigler,R. (1997) Dual-color fluorescence cross-correlation spectroscopy for multicomponent diffusional analysis in solution. *Biophys. J.*, **72**, 1878–1886.
54. Kettling,U., Koltermann,A. and Schwille,P. (1998) Real-time enzyme kinetics monitored by dual-color fluorescence cross-correlation spectroscopy. *Proc. Natl Acad. Sci. USA*, **95**, 1416–1420.
55. Enderlein,J., Ruckstuhl,T. and Seeger,S. (1999) Highly efficient optical detection of surface-generated fluorescence. *Appl. Opt.*, **38**, 724–732.
56. Ruckstuhl,T., Enderlein,J., Jung,S. and Seeger,S. (2000) Forbidden light detection from single molecules. *Anal. Chem.*, **72**, 2117–2123.